Study on the Annular Fluid Level Identification Algorithm for Ultra-Deep Wells Based on Acoustic Velocity Correction

Kerou Liu[1], Chao Yang[2], Mu Li[1], Shenyun Tang[3], Weiwei Hao[1,*], WeiWang[1], Yufei Chen[1] and Yafei Li[1]

[1] CNPC Engineering Technology R&D Company Limited, Beijing, 102206, China

[2] China Petroleum Technical Service Corporation Limited, Beijing, 100007, China

[3] China Petroleum Group Chuanqing Drilling Engineering Co., Ltd., Karamay, 841000, China

INFORMATION

Keywords:
Annular liquid level
sound velocity
temperature-pressure field
on-site test

DOI: 10.23967/j.rimni.2025.10.71070

SCIPEDIA Revista Internacional de Métodos Numéricos para Cálculo y Diseño en Ingeniería

Revista Internacional Métodos numéricos para cálculo y diseño en ingeniería RIMNI

In cooperation with CIMNE

Study on the Annular Fluid Level Identification Algorithm for Ultra-Deep Wells Based on Acoustic Velocity Correction

Kerou Liu[1], Chao Yang[2], Mu Li[1], Shenyun Tang[3], Weiwei Hao[1,*], Wei Wang[1], Yufei Chen[1] and Yafei Li[1]

[1]CNPC Engineering Technology R&D Company Limited, Beijing, 102206, China

[2]China Petroleum Technical Service Corporation Limited, Beijing, 100007, China

[3]China Petroleum Group Chuanqing Drilling Engineering Co., Ltd., Karamay, 841000, China

ABSTRACT

The geological conditions and pressure system of ultra-deep oil and gas wells are complex, and formation leakage conditions are prone to occur. Accurately obtaining the annular liquid level depth during leakage is crucial for treatment decisions. In the high-temperature and high-pressure wellbore environment of ultra-deep wells, the sound velocity shows a non-uniform variation trend, which seriously affects the accuracy of annular liquid level identification. Therefore, it is of significance to carry out a study on the annular fluid level identification algorithm based on acoustic velocity correction. Based on establishing a calculation model for the annular temperature and pressure field, a sound velocity calculation model in the annular air section was constructed. By combining the actual sound velocity of the clear signal segment identified through the echo signal, the basic parameters in the sound velocity calculation model can be calibrated to obtain the calibrated wellbore sound velocity distribution. Finally, tests were conducted on simulated well sites and noisy production wells to verify the accuracy of the annular liquid level identification algorithm constructed in this study. The results showed that the identification algorithm had an error of less than 2%. All in all, this study can effectively meet the demand for dynamic annular liquid level data during the leakage conditions, which is of great significance for the treatment and decision-making in deep and ultra-deep wells.

OPEN ACCESS

Received: 30/07/2025

Accepted: 25/09/2025

Published: 23/01/2026

DOI
10.23967/j.rimni.2025.10.71070

Keywords:
Annular liquid level
sound velocity
temperature-pressure field
on-site test

1 Introduction

The geological conditions and pressure system of ultra-deep oil and gas wells are complex, and they face complex environments such as high temperature, high pressure, and high production [1]. Under complex and multi-factor coupling conditions, the safety density window is extremely narrow, and overflow and leakage conditions are prone to occur, directly threatening the safety of drilling [2]. In the field of oil and gas production, annular liquid level monitoring mainly provides a basis for oil production strategies [3], thereby improving the optimal pumping state [4]. The main methods include acoustic, radar, laser, and fiber optic liquid level measurement [5]. In the field of drilling, annular liquid level monitoring is mainly carried out under leakage conditions, mainly using acoustic methods [6].

*Correspondence: Weiwei Hao (haowwdr@cnpc.com.cn).

When leakage occurs, the liquid level in the annulus is located below the wellhead, and the liquid level changes frequently [7], which puts higher demands on the annulus liquid level identification algorithm. However, at present, there are two key issues in the acoustic methods, including the uncertainty of downhole sound velocity and the difficulty in extracting echo characteristics. Among them, the sound velocity underground can be affected by the pressure and temperature of the propagation medium, resulting in changes. And the extraction of echo features is affected by noisy environments, which can cause distortion or even masking of echo features, making it difficult to accurately calculate the depth of the annular liquid surface.

Researchers have proposed corresponding solutions to improve the accuracy of annular liquid level measurement in response to the above-mentioned problems. Kan et al. [8] performed a Fourier transform on the original signal and then used Wavelet Domain Denoising (WDD) to obtain clearer liquid level echoes. Zhang et al. [9] used time series analysis and innovative adaptive Kalman filtering methods to achieve high-precision measurement and noise processing of liquid level echoes. Zhou et al. [10] used the resonant frequency difference (RFD) of the resonant acoustic signal in annular to calculate the dynamic liquid level. The above methods focus on the processing of echo signals, but ignore the uncertainty of sound velocity in the annular space of the wellbore. Based on considering the variation of sound velocity, Wu et al. [11] proposed the All-Phase Fast Fourier Transform (apFFT), which calculates the average sound velocity underground through the frequency spectrum and phase spectrum of the signal, improves the spectral leakage ability, and enhances the accuracy of sound velocity calculation. Liang et al. [12] proposed a predictive model for predicting liquid level depth by integrating multi-channel liquid level positions based on an improved short-time energy zero crossing function and a three-electric-center clipping function. However, the model lacks actual data samples for validation. Wang et al. [13] used a Butterworth Low-Pass Filter (BLPF) and AMDF to extract the average period of the echo signal and calculate the downhole sound velocity. They also used WDD and Wavelet Singular Value Detection (WSVD) to calculate the depth of the liquid level. However, they did not consider the overlap between the liquid level echo and the drill pipe coupling echo in shallow wells, and manual selection of the liquid level echo signal was required. In addition, physics-informed machine learning, deep learning architectures, and Bayesian fusion techniques have been successfully implemented in analogous high-noise and complex thermodynamic wellbore environments [14]. Roy et al. [15] used the Artificial Neural Network (ANN) model to cascade it with the frequency to voltage converter to achieve a higher accuracy level measurement. Bagheri et al. [16] achieved classification and prediction of aperture distribution in the complex lithology through a two-step deep learning algorithm. However, there are very few related intelligent algorithm research on the correction of sound speed in annular liquid level identification.

In summary, current research mainly relies on signal processing, with insufficient consideration of wellbore temperature and pressure fields. However, the speed of sound changes when the temperature and pressure change, which can cause inaccurate identification of liquid level. Especially in deep and ultra-deep wells, the temperature, pressure and length of the annular air section are larger, which further limits the improvement of the recognition accuracy. Therefore, it is of great significance to correct the sound velocity by considering the annular temperature-pressure field, which can effectively improve the accuracy of annular liquid level monitoring.

In this study, an echo signal processing algorithm was constructed first, which includes echo signal preprocessing, echo signal reconstruction, and echo feature extraction. Meanwhile, the processing results of typical echo signals are presented at each step, which helps to explain the purpose and function of the algorithm. Finally, simulated wellsite testing and noisy production well testing were conducted, representing the annular liquid level in the shallow well section and the deep well section,

respectively. Combined with a large number of on-site tests, the accuracy of the algorithm established was ultimately verified. In summary, this study can improve the accuracy of liquid level echo identification by establishing a sound velocity calibration algorithm, which can provide guarantees for the safe handling of drilling well leakage conditions and support the safe drilling of deep and ultra-deep wells.

2 Echo Signal Processing Algorithm

The processing of annular liquid level echo signals can be divided into signal preprocessing, signal reconstruction, and feature extraction, as shown in Fig. 1. In the signal preprocessing stage, the signal is first decomposed into Intrinsic Mode Function (IMF) [17] components using the Spectral Variation Mode Decomposition algorithm (SVMD) [18]. Then, the original echo signal and IMF component signal are converted into time-frequency spectra through S-transformation. In the signal reconstruction stage, the above two signals are first subjected to similarity analysis, and then high-frequency noise signals are removed. Then, low-frequency IMFs below the similarity threshold are reconstructed to form a new signal with clearer data and more distinct features. In the feature extraction stage, the first step is to locate the position of the liquid surface echo signal using the Holtling's T^2 test method. Then, the echo signal of the drill pipe coupling is extracted using the short-time Autocorrelation Function (ACF) [19] and the Average Amplitude Difference Function (AMDF) [20], and the acoustic velocity of the wellbore section with obvious coupling signal characteristics is obtained. For sections with unclear drill pipe coupling signals, it is necessary to use calibration algorithms to supplement the sound velocity. The sound velocity calibration algorithm used in this study comprehensively considers the effects of temperature, pressure, and humidity in the annulus, and can achieve higher accuracy in calculating the liquid level height in the annulus.

2.1 Characteristics of Echo Signal

The original echo signal consists of the detonation signal, drill pipe coupling echo signal, liquid surface echo signal, and secondary echo signal. Among them, the detonation wave is located in the early stage and has a significantly larger amplitude than other signals. Due to the uniform distribution and consistent length of drill pipe couplings, the drill pipe coupling echo signal appears as a periodic signal. During the downward propagation, the intensity of the sound waves will attenuate. Therefore, the shallower the depth, the stronger the signal reflected by the drill pipe coupling, and the stronger the signal reflected by the liquid surface. When the liquid surface is at a deeper position, the receiver can receive clearer liquid surface echo signals. If the liquid level is shallow, the echo signal may be covered by the drill pipe coupling echo signal due to its low intensity.

The typical original echo signal and its time-frequency spectrum measured by the acoustic methods are shown in Fig. 2. The signal contains two dominant frequencies, with the low-frequency part dominant at 18 Hz, which is the frequency of the drill pipe coupling echo signal, and the high-frequency part dominant at 180 Hz, which is the frequency of sound wave propagation (Fig. 3).

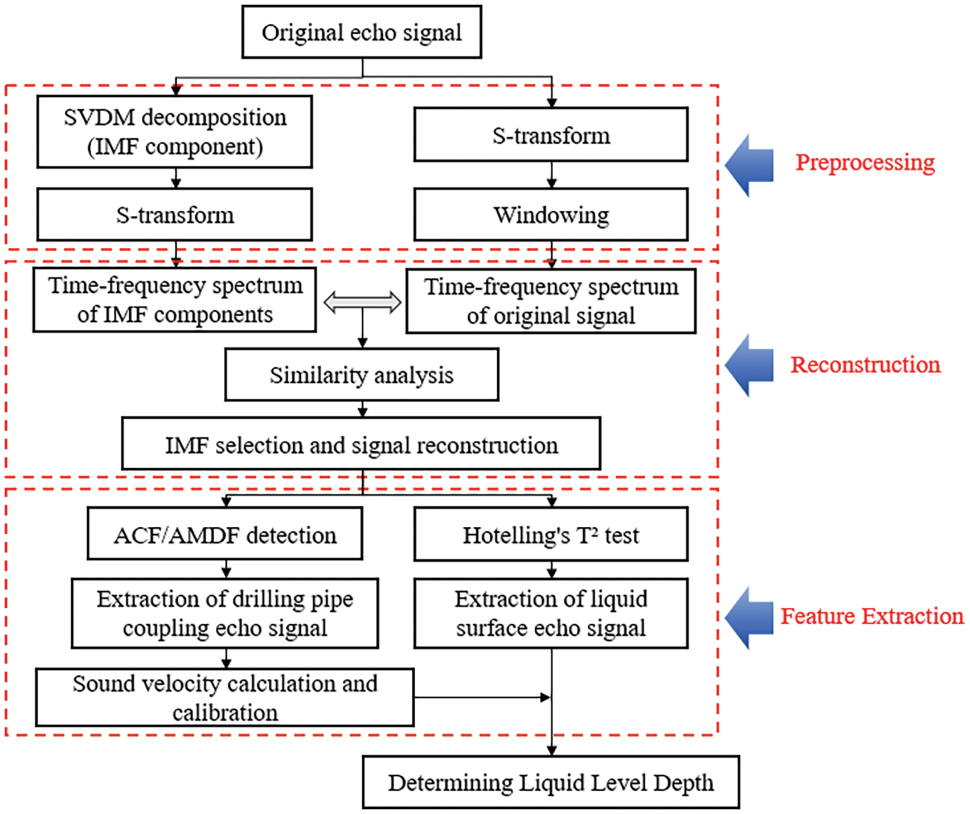

Figure 1: Annular liquid level echo signals processing flow

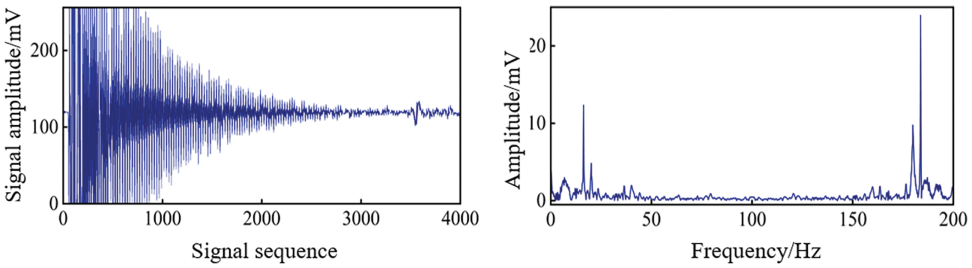

Figure 2: Typical liquid level echo signal in shallow well section. (**a**) Echo signal; (**b**) Echo signal frequency spectrum

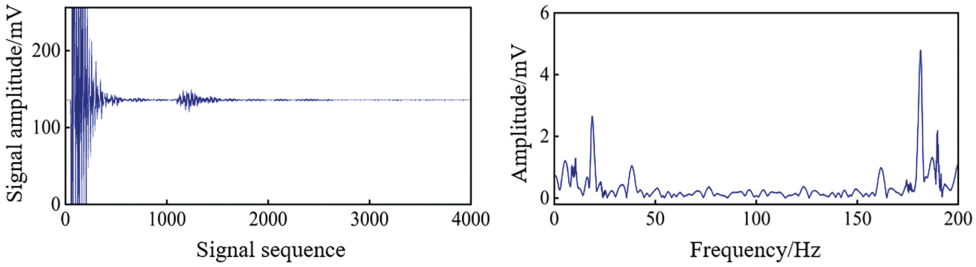

Figure 3: Typical liquid level echo signal in deep well section. (**a**) Echo signal; (**b**) Echo signal frequency spectrum

2.2 Signal Preprocessing

2.2.1 Original Signal Decomposition

The high-frequency noise in the original echo signal has obvious periodicity and can cause significant interference to the detection of the drill pipe coupling echo signal. To determine the clear position of the drill pipe coupling echo, it is necessary to filter out the high-frequency signal while preserving the low-frequency effective information as much as possible. Modal decomposition can decompose a single signal into multiple frequency bands, and then perform time-frequency analysis based on the decomposed signal and the effective signal that needs to be resolved. Finally, the component signals that meet the similarity requirements can be reconstructed to obtain a new signal. In this study, the SVMD method is used to decompose the original echo signal into the sum of IMFs. This method is an adaptive and quasi-orthogonal signal decomposition method that can adaptively achieve modal decomposition without pre-set modal numbers, with low computational complexity and high robustness. Specifically, the penalty parameter was set to 2000. The iterations stop when the relative change between two successive updates falls below 1×10^{-6}, or when the maximum number of iterations reaches 500, whichever occurs first. To further enhance repeatability in the stochastic components of SVMD, the random seed was fixed at 42. Due to the maturity of the SVMD algorithm, it will not be presented in detail here.

2.2.2 S-Transformation

Time-frequency spectrum similarity can describe the changes in frequency components of two signals in the time domain, which can solve the problem of non-stationary signals constantly changing in frequency in the time domain. And it can also effectively reflect the correlation between two non-stationary signals. Through the S-transform, the energy distribution of a signal can be observed simultaneously in both the time and frequency domains. Meanwhile, the S-transform can maintain a direct relationship with the Fourier transform while also having different resolutions at different frequencies.

In this study, the S-transform was used to obtain the time-frequency spectrum of the original echo signal X^{t-f} and each IMF component S_i^{t-f}. Due to the slower attenuation of low-frequency signals compared to high-frequency signals, the distribution range of low-frequency components in the original signal is larger from the perspective of the sampling sequence. The distribution range of high-frequency components is relatively small, but the overall amplitude is much higher than that of low-frequency components, and then rapidly decays. Due to the strong amplitude characteristics of

high-frequency sound waves, the high-frequency components have higher periodicity, which affects the detection results of the drill pipe coupling echo signal period. Therefore, to filter out high-frequency signals and highlight the periodic characteristics of low-frequency signals, it is necessary to perform windowing on the time-frequency spectrum of the original signal. The window function is shown in Eq. (1).

$$\hat{X}^{t-f}(j) = \begin{cases} X^{t-f}(j), & f = 0 : f_{\max}/2 \\ 0, & otherwise \end{cases} \tag{1}$$

where $\hat{X}^{t-f}$ is the windowed time-frequency spectrum, $f_{\max}$ is the signal sampling frequency, and f is the windowed signal frequency. Compare the windowed time-frequency spectrum with the time-frequency spectrum of each IMF component, and the similarity S_{im} can be expressed as follows.

$$S_{im} = \frac{1}{K} \sum_{j=1}^{K} \left| \hat{X}^{t-f}(j) - S_i^{t-f}(j) \right| \tag{2}$$

where K is the total number of modes. The closer S_{im} is to 0, the higher the similarity and stronger the correlation between the two. Taking the typical echo signal in the deep well section as an example (Fig. 2), the windowed time-frequency spectrum of the original signal is shown in Fig. 4, and the time-frequency spectrum of the IMF component is shown in Fig. 5. It can be seen that the first 7 IMF components are mainly distributed in the low-frequency range, with a high similarity to the drill pipe coupling echo signal frequency. The last 9 IMF components are mainly distributed in the high-frequency range, with a higher similarity to the high-frequency sound wave propagation frequency.

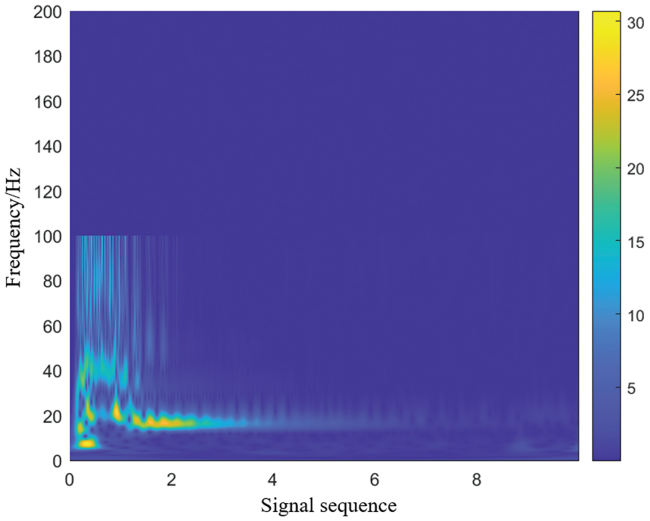

Figure 4: Windowed time-frequency spectrum of the original signal

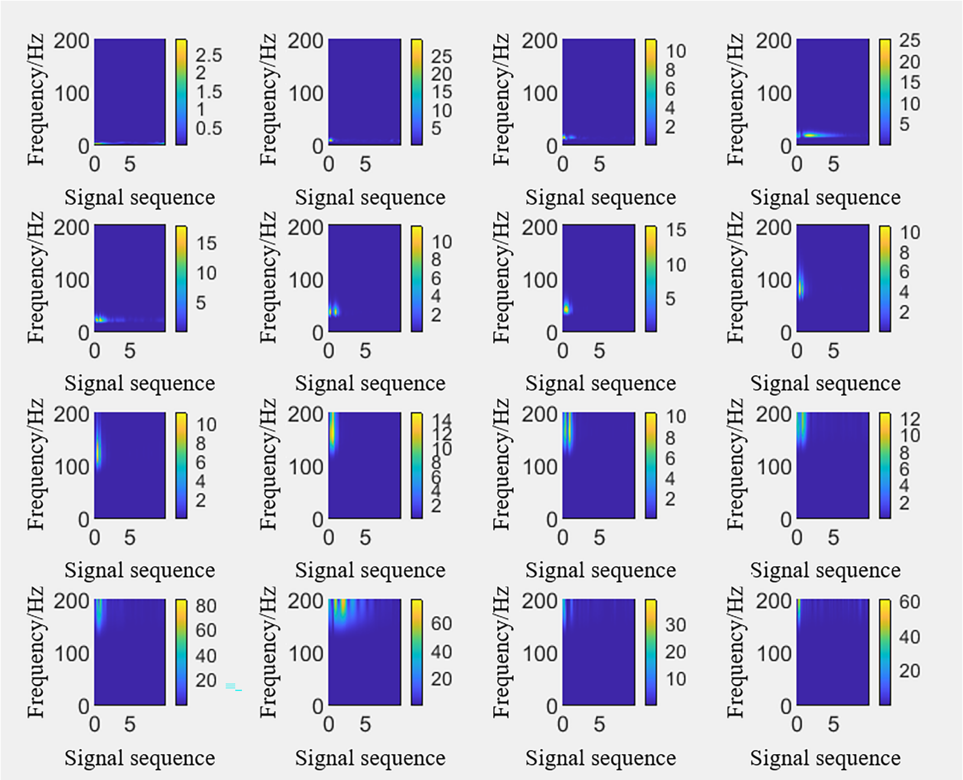

Figure 5: Time-frequency spectrum of IMF components

2.3 Signal Reconstruction

The IMF component with the smallest similarity indicates that it has the highest similarity with the low-frequency band of the original echo signal, and the drill pipe coupling echo signal period at this frequency is closer to the actual period. Due to the increasing temperature and pressure in the annulus with the depth of the well, the downhole sound velocity shows a gradually increasing trend, resulting in an increase in the drill pipe coupling echo signal period. To obtain a more accurate period, the IMF component with the highest similarity is positioned, and the largest similarity among the two adjacent IMF components is selected as the threshold. All IMF components with similarity less than the threshold are reconstructed to obtain a new echo signal.

Taking the typical echo signal in the deep well section as an example (Fig. 2), the similarity between the time-frequency spectrum of each IMF component and the windowed of the original signal was further calculated, and the results are shown in Fig. 6. Finally, 1.9827 was selected as the similarity threshold, and the reconstructed echo signal is shown in Fig. 7.

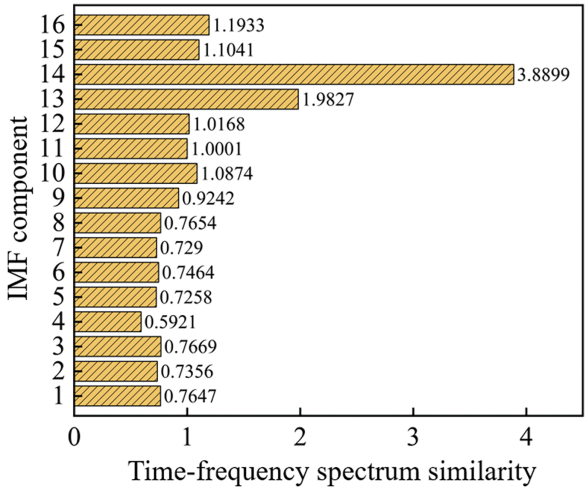

Figure 6: Time-frequency spectrum similarity of IMF components

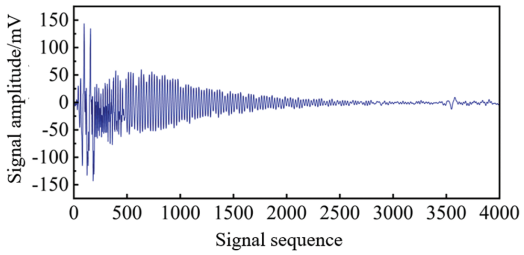

Figure 7: Reconstructed echo signal

2.4 Feature Extraction

2.4.1 Extraction of Coupling Wave Signal

Since the drill pipe coupling echo signal is a signal with quasi-periodic characteristics, some methods in speech signal fundamental period detection can be referred to, such as period estimation based on non-parametric statistics, autocorrelation function, average amplitude difference function, and other period extraction functions to estimate the period. Their essence is based on the assumption that there must be some similarity between the sample sets sampled with period length to calculate the signal period. The ACF method is similar in concept to the AMDF method, both of which measure the similarity between the original signal and its shifted signal. In this study, the AMDF method was mainly used, and the ACF method was used as an auxiliary method to effectively reduce noise interference and improve the accuracy of echo period extraction. The formula is as follows.

$$C_A(l) = \sum_{n=0}^{N-l-1} \frac{s(n)\, s(n+l)}{|s(n+l) - s(n)|} \tag{3}$$

where N is the frame length of the signal, l is the time delay, n is the signal sequence, $s(n)$ is the signal amplitude. Taking the typical echo signal in the deep well section as an example (Fig. 2), the ACF/AMDF detection results are shown in Fig. 8. By reading the number of signal sampling frames and sampling frequency between two peaks, combined with the drill pipe coupling spacing data, the sound velocity distribution in the annulus can be calculated.

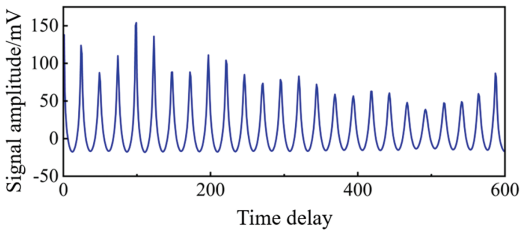

Figure 8: ACF/AMDF detection results

2.4.2 Sound Velocity Calibration Algorithm

Due to the influence of underground temperature, pressure, and humidity on sound velocity, and limited sampling frequency, it is difficult to ensure accurate reading of sound velocity data for all annular sections. Therefore, it is necessary to construct annular temperature and pressure field models, and calibrate the model parameters in real time based on the sound velocity data of the clear data segment, in order to calibrate the sound velocity data of all annular segments.

Sound Velocity Extraction of Clear Signal

After extracting the position of the dilling coupling signal point, the average sound velocity between adjacent coupling points can be calculated. The formula is as follows.

$$c_i = \frac{2 \times L \times f_s}{n_{i+1} - n_i} \tag{4}$$

where c_i is the average sound velocity between the i-th and the next drill pipe coupling, L is the length of a section of drill pipe, generally 9.6 m, f_s is the sampling frequency, and n_i representing the sampling point of the i-th coupling. In traditional algorithms, the acoustic wave velocities are always directly obtained by calculating the average sound velocity, which leads to a certain error in the calculation results. In this study, a more accurate sound speed calculation model is built, which can provide strong support for the accurate improvement of liquid level recognition.

Calculation of Sound Velocity in the Annular Section

The relationship between the speed of sound c and temperature T, pressure P, and humidity can be expressed as follows [21].

$$\begin{cases} c = \sqrt{\dfrac{\gamma Z R (T + 273.15)}{M_a \left[1 - x_w \left(1 - \dfrac{M_w}{M_a}\right)\right]}} \\ x_w = \dfrac{0.01 RHf P_{sv}}{P} \end{cases} \tag{5}$$

where γ is the specific heat ratio, P is atmospheric pressure, Pa, ρ is air density, kg/m^3, M_a is the molar mass of dry air, kg/mol, M_w is the molar mass of water vapor, kg/mol, x_w is the mole fraction of water vapor [22], Z is the compressibility factor, related to temperature and pressure, R is the universal gas constant, 8.3144598 J/(mol·K), RH is the relative humidity, %. It can be seen that as the temperature increases, the speed of sound becomes faster. As the pressure increases, the speed of sound slows down.

In this study, the influence of annulus temperature and pressure on sound velocity is mainly considered, therefore it is necessary to calculate the temperature and pressure fields inside the annulus.

During the drilling process, the drilling fluid first passes through the drill pipe at temperature T_1, flows through the bottom of the well, absorbs formation heat, and returns to the surface at T_2. This flow and heat transfer process has a significant impact on the performance of drilling fluid and the distribution of wellbore pressure. In the case of wellbore leakage, some of the drilling fluid is lost to the formation, causing a decrease in the liquid level at the wellhead of the annulus and the invasion of air. It has an additional impact on the heat transfer process, changing the thermal equilibrium state inside the wellbore. Therefore, the effects of air intrusion and liquid level changes on fluid thermodynamic properties and heat transfer characteristics need to be considered in flow and heat transfer models. Ultimately, the temperature gradient of the wellbore annulus air can be obtained.

• Heat transfer model

In accordance with actual construction conditions, the following assumptions are proposed to simplify the calculation: (1) The heat exchange in the axial direction of the formation is ignored, (2) The physical parameters (density, specific heat capacity, etc.) of drill pipe, casing, and formation rock are not affected by temperature and pressure, (3) The heat exchange in the radial direction of the drilling fluid is ignored, since axial convective transfer dominates during leakage, (4) The wellbore is a concentric circular structure, (5) The geothermal gradient remains constant. Finally, the diagram of the wellbore fluid flow and heat transfer model under leakage conditions is shown in Fig. 9.

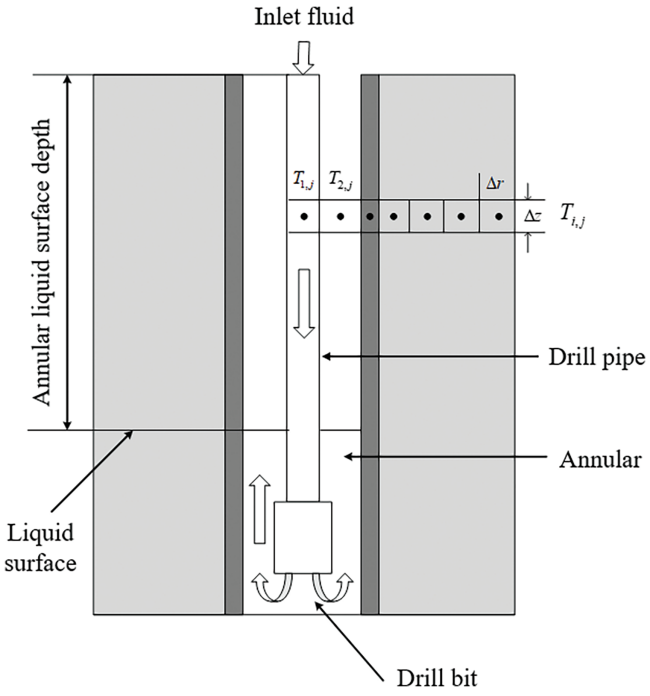

Figure 9: Diagram of the wellbore fluid flow and heat transfer model under leakage conditions

According to the law of energy conservation, the sum of the energy entering the control body from the outside dQ and the work done by the outside on the control body dw is equal to the increment of energy inside the control body dE, which can be expressed as follows.

$$\mathrm{d}Q + \mathrm{d}w = \mathrm{d}E \tag{6}$$

Due to the formation of U-shaped pipes in the wellbore during the shutdown period, air and fluid components are generated in both the drill pipe and annulus. Therefore, the energy changes of the control body are calculated separately for the drill string and annulus, and the energy changes of drilling fluid and air are considered separately.

During the process of drilling fluid flowing from the wellhead into the wellbore, the energy changes of the control body are mainly reflected in: (1) The convective heat transfer between the fluid in the drill pipe and the annulus, (2) The net heat flowing vertically into the control body, (3) The heat generated by fluid flow and rock breaking by drill bit, (4) The internal energy change of the internal control system per unit time, as shown in Fig. 10.

$$2\pi r_{pi} U\left[\left(T_a(z,t) - T_p(z,t)\right)\right] - \rho_m q C_m \frac{\partial T_p}{\partial z} + Q_s = \rho_m C_m \frac{\partial T_p(z,t)}{\partial t} \pi r_{pi}^2 \tag{7}$$

where T_p is the temperature of the fluid inside the annulus, °C, T_a is the fluid temperature inside the drill pipe, °C, z is depth, t is time, r_{pi} is the inner radius of the drill pipe (excluding wall thickness), m, C_m is the specific heat capacity of the drilling fluid, J/ (kg·°C), U is the total convective heat transfer coefficient between the fluid inside the drill pipe and the annulus, W/ $\left(m^2 \cdot °C\right)$, Q_s is other heat sources, W/ $\left(m^2 \cdot °C\right)$, ρ_m is drilling fluid density, kg/m^3, q is drilling fluid displacement, kg^3/s.

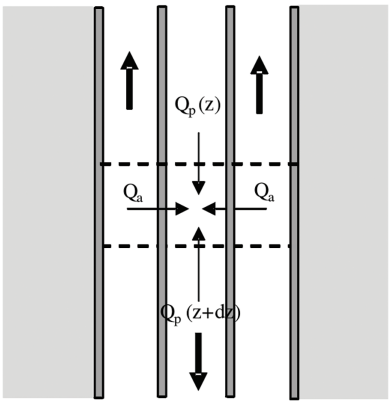

Figure 10: Diagram of drilling fluid control body energy change in the drill pipe

The energy changes of the control body in the air part of the drill pipe are mainly reflected in: (1) The convective heat transfer between the fluid in the drill pipe and the annulus, (2) The internal energy change of the internal control system per unit time, as shown in Fig. 11.

$$2\pi r_{pi} U\left[\left(T_a(z,t) - T_p(z,t)\right)\right] - \rho_m q C_m \frac{\partial T_p}{\partial z} + Q_s = \rho_m C_m \frac{\partial T_p(z,t)}{\partial t} \pi r_{pi}^2 \tag{8}$$

where T_{pk} is the temperature of the air inside the annulus, °C, T_{ak} is the air temperature inside the drill pipe, °C, C_{air} is the specific heat capacity of air, J/ (kg·°C), ρ_{air} is air density, kg/m^3.

During the process of drilling fluid flowing from the bottom wellbore to the wellhead in the annulus, the energy changes of the control body are mainly reflected in: (1) The convective heat transfer between the fluid in the annulus and the drill pipe, (2) The convective heat transfer between the fluid in the annulus and the boundary of the formation, (3) The net heat flowing vertically into the control body, (4) The heat generated by fluid flow and rock breaking by drill bits, (5) The internal energy change of the internal control system per unit time, as shown in Fig. 12.

$$-\rho_m q C_m \frac{\partial T_a(z,t)}{\partial t} + 2\pi r_{po} h\left[\left(T_f(z,t) - T_a(z,t)\right)\right]$$
$$-2\pi r_{pi} h\left[\left(T_a(z,t) - T_p(z,t)\right)\right] = \rho_m C_m \frac{\partial T_a(z,t)}{\partial t}\pi\left(r_w^2 - r_{po}^2\right) \quad (9)$$

where T_f is the wellbore temperature, °C, r_{po} is the outer diameter of the drill pipe, m, r_w is the diameter of the wellbore, m, h is the convective heat transfer coefficient between the annular fluid and the wellbore wall.

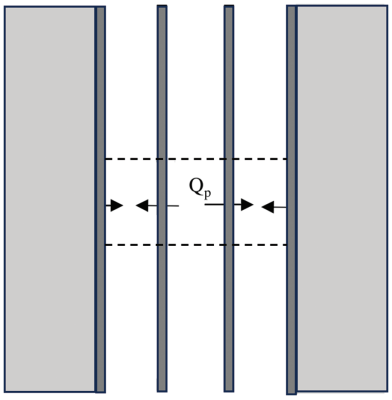

Figure 11: Diagram of air control body energy change in the drill pipe

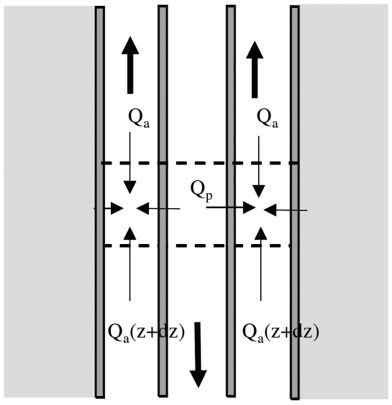

Figure 12: Diagram of drilling fluid control body energy change in the annular

The energy changes of the air control body in the annulus are mainly reflected in: (1) The convective heat transfer between the fluid in the annulus and the drill pipe, (2) The convective heat transfer between the fluid in the annulus and the boundary of the formation, (3) The internal energy change of the internal control system per unit time, as shown in Fig. 11.

$$Q_{air} + 2\pi r_{po} h_{a-f}\left[\left(T_f(z,t) - T_{ak}(z,t)\right)\right]$$
$$-2\pi r_{pi} h_{a-p}\left[\left(T_{ak}(z,t) - T_{pk}(z,t)\right)\right] = \rho_{air} C_{air} \frac{\partial T_a(z,t)}{\partial t}\pi\left(r_w^2 - r_{po}^2\right) \quad (10)$$

where Q_{air} represents the change in heat inside the air, $\mathrm{W}/\left(\mathrm{m}^{2\cdot\circ}\,\mathrm{C}\right)$, a represents annulus, f represents formation, and h_{a-f} is the heat transfer coefficient from the annulus to the formation.

• Initial and boundary conditions

The outlet temperature of the annulus is known as follows.

$$T_a(z=0,t) = T_{out} \tag{11}$$

At the bottom of the well, the temperature of the drilling fluid inside the drill pipe is equal to the temperature of the drilling fluid in the annulus, as shown in Eq. (12).

$$T_p(z=H,t) = T_z(z=H,t) \tag{12}$$

The formation changes linearly at an infinite distance from the wellbore, as shown in Eq. (13).

$$T_f(z, r\to\infty, t) = T_s + zT_g \tag{13}$$

• Annular pressure model

The gas pressure in the sealed annulus can be calculated using the energy equation.

$$\frac{dP}{dz} = \rho_{air} g \tag{14}$$

where ρ_{air} is the gas density in the annulus. Under the known temperature gradient in the wellbore annulus, ρ_{air} can be obtained from the following formula based on the gas state equation.

$$\rho_{air} = \frac{PM_{air}}{ZRT} \tag{15}$$

According to the equation, the pressure distribution of the annular gas can be obtained by integrating from the top to the bottom of the wellbore section at depth, as shown in Eq. (16).

$$P_{out} = P_{in} \cdot e^{\frac{M_{air} g \Delta z}{ZRT}} \tag{16}$$

Model Solution

Taking the typical echo signal in the deep well section as an example (Fig. 2), the selected clear segment signal is shown in Fig. 13.

In this study, the finite difference scheme is mainly used to discretize the constructed model in space and time, and then the differential equations are processed using a more stable fully implicit scheme, and the model is solved through numerical methods. Among them, the first-order spatial derivative in the control equation adopts a two-point backward difference format, the first-order time derivative adopts a two-point forward difference format, and the second-order spatial derivative adopts a three-point center difference format. In terms of grid division, a grid is divided every 30° in radial direction and every 9.6 m in longitudinal direction (consistent with the length of a single drill pipe). Due to the use of implicit differences, the time step is set to 1 s. For a wellbore with a relative humidity of 0%, the temperature, pressure, and sound velocity changes in the annulus are shown in Fig. 14. It can be seen that as the well depth increases, the annular temperature, pressure, and sound velocity all show a linear upward trend.

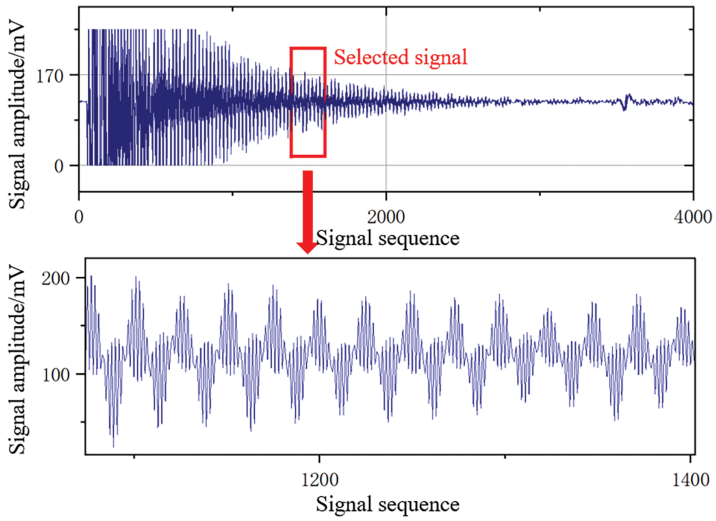

Figure 13: Selected clear segment signal

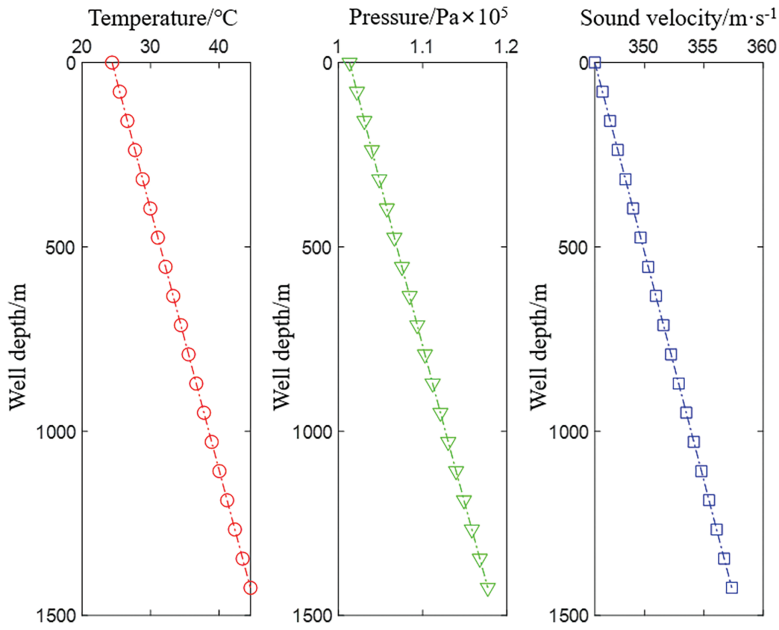

Figure 14: Changes in temperature, pressure, and sound velocity within the annulus

2.4.3 Extraction of Liquid Surface Echo Signal

In an ideal situation, the liquid surface echo signal can exhibit different characteristics from the drill pipe coupling echo signals, making it easy to determine the propagation time of the echo in the annulus. However, in actual wellbore environments, both downhole noise and secondary echo signals can interfere with the liquid surface echo signal, making it difficult to distinguish the liquid surface position and thus affecting the accuracy of measurement results. Therefore, the Holtling's T^2 test method was used to detect signal mutation points and obtain the liquid surface position. This method

assumes two sets of data, namely offline data without liquid surface echo signals y_i and online data with liquid surface echo signals y_k Firstly, calculate the mean and variance of offline data.

$$\overline{y}_N = \frac{1}{N}\sum_{i=1}^{N} y_i \tag{17}$$

$$\hat{\Sigma} = \frac{1}{N-1}\sum_{i=1}^{N} \left(y_i - \overline{y}_N\right)\left(y_i - \overline{y}_N\right)^{\mathrm{T}} \tag{18}$$

where N is the number of offline data samples, $\overline{y}_N$ is the sample mean, $\hat{\Sigma}$ is the sample mean square error. Based on the mean and variance of the signal segment corresponding to the current signal point, the test statistic for the current signal point can be determined. The test statistic is defined as follows.

$$J = \left(\overline{y}_N - y_k\right)^{\mathrm{T}} \hat{\Sigma}^{-1} \left(\overline{y}_N - y_k\right) \tag{19}$$

Take the signal points with a test statistic greater than the threshold of the statistic as the feature points of the liquid surface echo signal. The threshold for calculating statistical measures is as follows.

$$J_{th,T^2} = \frac{m\left(N^2-1\right)}{N\left(N-m\right)} F_{\lambda}\left(m, N-m\right) \tag{20}$$

where λ is the acceptable false alarm rate, $F_{\lambda}\left(m, N-m\right)$ is the F-distribution [23] with degrees of freedom m and $N-m$, m represents the degree of freedom of the system, and is set to 1 during filtering.

$$\begin{cases} J \le J_{th,T^2} \Rightarrow \text{Not reaching the liquid surface echo signal} \\ J \ge J_{th,T^2} \Rightarrow \text{Reaching the liquid surface echo signal} \end{cases} \tag{21}$$

By combining the sound velocity calibration algorithm to obtain the annular sound velocity distribution, the annular liquid surface depth can be accurately calculated. Taking the typical echo signal in the deep well section as an example (Fig. 2), the acceptable false alarm rate λ is set to 0.01, and the threshold is calculated to be 6.967. It should be noted that many factors affect the form of the echo signal, which results in the above parameters that need to be corrected for each well. Because the signal points that actually represent liquid level echoes are relatively concentrated and have a larger value, the available values for the above parameters are relatively large, so they can be automatically calibrated in software programming based on the number of values exceeding the threshold. Detect the echo signal sampling sequence, and the position where the threshold is first exceeded in the distribution is the liquid surface echo signal position, as shown in Fig. 15.

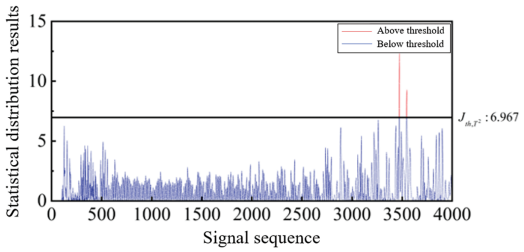

Figure 15: Holtling's T^2 test results in the deep well section

3 Field Experimental Testing

3.1 Simulated Wellsite Test

The self-developed equipment was used for testing in the Bohai drilling experimental well. During the testing, the annular pressure was 0 MPa, and the actual liquid surface depth was 580 m. A total of 10 measurements were carried out, and the measurement results are shown in Fig. 16. Among them, Fig. 16a shows the original echo signal data, and Fig. 16b shows the preprocessed echo signal. The final identified average annular liquid surface depth is 580 m, which is consistent with the actual depth, demonstrating the accuracy of the algorithm in this paper.

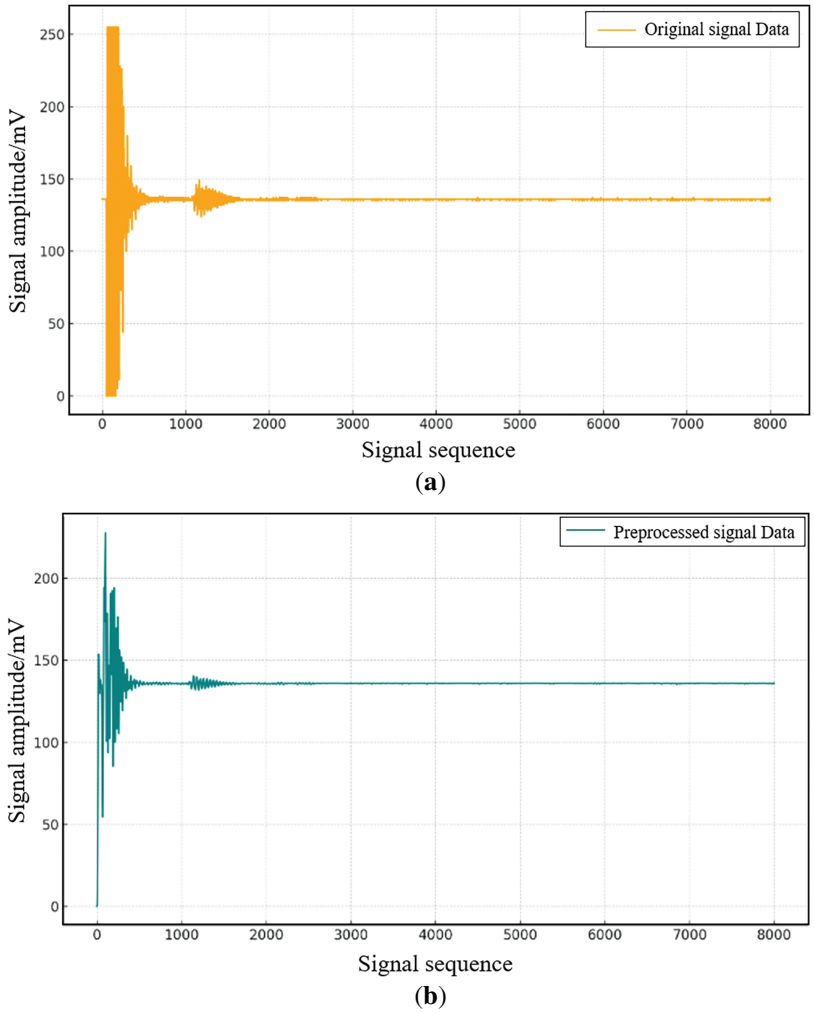

Figure 16: Test result in the Bohai drilling experimental well. (**a**) Original echo signal data; (**b**) Preprocessed echo signal

3.2 Noisy Production Well Test

Tests were conducted in the production well in Dagang Oilfield. The environment and underground working conditions can cause echo signals to contain noise, and the production well is accompanied by serious noise, which has affected normal liquid level measurement work. This test is

based on the existing measuring equipment. The conventional measurement annular liquid level depth in the well is 700 m. Based on the algorithm established in this study, the echo signals were processed to obtain the actual liquid level depth of 108 m (Fig. 17), indicating that the developed algorithm can eliminate interference in the face of a large amount of noise, and quickly and accurately complete measurement work.

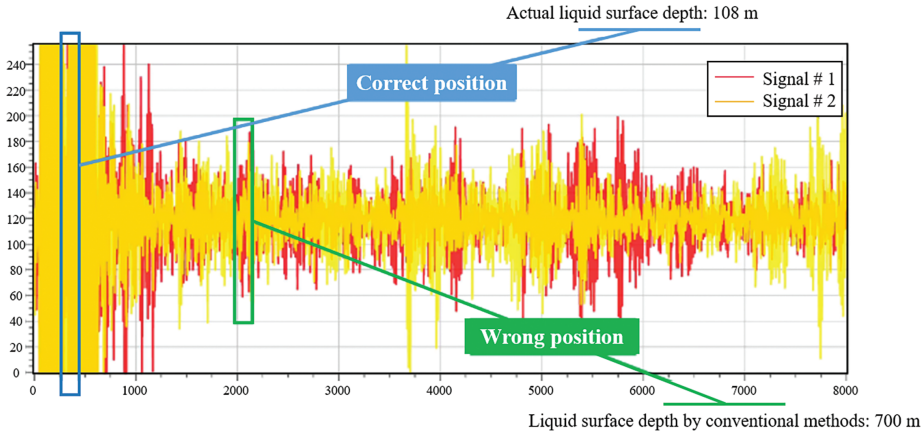

Figure 17: Test result in the production well in Dagang Oilfield

3.3 Summary of Test Results

In addition to the simulated wellsite test representing the deep well sections and the noisy production well test representing shallow well sections mentioned above, the algorithm established in this study has also undergone multiple tests, and the statistical results are shown in Fig. 18. The results showed that the reference value error is less than 2%, indicating that the algorithm established in this study can effectively reflect changes in liquid level depth.

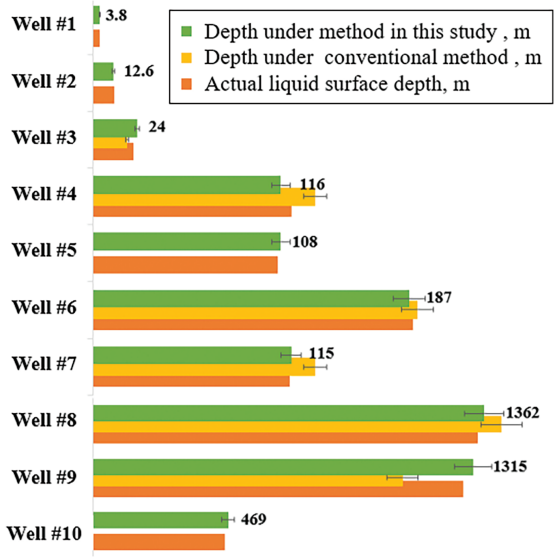

Figure 18: Test result in production well in Dagang Oilfield

4 Conclusion

(1) Based on considering the influence of the temperature and pressure environment in the annulus on sound velocity, an ultra-deep well annular fluid level identification algorithm that can correct sound velocity in real time was constructed in this study. It includes signal preprocessing, signal reconstruction, and feature extraction, which can effectively improve the accuracy of annulus liquid surface identification.

(2) Based on the constructed annular temperature and pressure field model, a sound velocity calibration algorithm for the annular air section was developed. By calculating the sound velocity of the clear section of the drill pipe coupling echo signal, the model parameters can be calibrated, and further calculations can be made to obtain the sound velocity distribution of the entire annular air section, helping to obtain more accurate liquid surface depth.

(3) Simulated wellsite test and noisy production well test were conducted, representing the shallow well sections and deep well sections, respectively. Based on extensive on-site testing, the measurement error of the algorithm established in this study is less than 2%.

Acknowledgement: Not applicable.

Funding Statement: This research was funded by the National Key Research and Development Program of China (2023YFC3009200), the National Science and Technology Major Project (Grant No. 2025ZD1401905).

Author Contributions: The authors confirm contribution to the paper as follows: Performed the experiments, Kerou Liu; revised the manuscript, Chao Yang; analyzed the data, Mu Li; developed the methodology, Shenyun Tang; provided technical support, Weiwei Hao; conducted the simulations, Wei Wang; collected the samples, Yufei Chen; supervised the project, Yafei Li. All authors reviewed the results and approved the final version of the manuscript.

Availability of Data and Materials: The data that support the findings of this study are available from the Corresponding Author, Weiwei Hao, upon reasonable request.

Ethics Approval: Not applicable.

Conflicts of Interest: The authors declare no conflicts of interest to report regarding the present study.

References

1. He D, Jia C, Zhao W, Xu F, Luo X, Liu W, et al. Research progress and key issues of ultra-deep oil and gas exploration in China. Pet Explor Dev. 2023;50(6):1333–44. doi:10.1016/S1876-3804(24)60470-2.
2. Wang H, Huang H, Bi W, Ji G, Zhou B, Zhuo L. Deep and ultra-deep oil and gas well drilling technologies: progress and prospect. Nat Gas Ind B. 2022;9(2):141–57. doi:10.1016/j.ngib.2021.08.019.
3. Shinyakov J, Sukhorukov M, Torgaeva D, Soldatov A, Shalyapina N, Li D. Analysis of methods for measuring the liquid level in the annular space of an oil well. MATEC Web Conf. 2018;158:01029. doi:10.1051/matecconf/201815801029.
4. Srivastava M, Ali AA, Alshehhi AS, Kumar A, Spuskanyuk O, Abdulhai WM, et al. A systematic approach to monitoring and management of annulus pressures. In: Proceedings of the SPE/IADC Middle East Drilling Technology Conference and Exhibition; 2018 Jan 29–31; Abu Dhabi, United Arab Emirates. Houston, TX, USA: SPE; 2018. D031S015R003. doi:10.2118/189412-MS.

5. Haavik KE. Annuli liquid-level surveillance using distributed fiber-optic sensing data. SPE J. 2024;29(2):1195–209. doi:10.2118/217989-PA.
6. Li T, Wang Z, Gu YJ, Wang R, Wang Y. Experimental study of fracture structure effects on acoustic logging data using a synthetic borehole model. J Pet Sci Eng. 2019;183:106433. doi:10.1016/j.petrol.2019.106433.
7. Yang S, Fu J, Zhao N, Xu C, Han L, Wang J, et al. Comprehensive analysis of the annulus pressure buildup in wells with sustained gas leakage below the liquid level. Processes. 2024;12(12):2631. doi:10.3390/pr12122631.
8. Kan L, Gao B, Liang H, Lu Q, Guo J. Application of wavelet denoising in oil well dynamic liquid level monitoring. Control Instrum Chem Ind. 2014;41(9):1009–11. (In Chinese).
9. Zhang P, Yang Y, Fan F, Chang J. Study of oil well remote monitoring system based on ultrasonic distance measurement and cloud testing. Comput Meas Control. 2015;23(06):1907–11. (In Chinese).
10. Zhou W, Liu J, Gan L. Dynamic liquid level detection method based on resonant frequency difference for oil wells. Turk J Electr Eng Comput Sci. 2018;26(6):2967–75. doi:10.3906/elk-1805-68.
11. Wu J, Wang K, Liu Y, Gao J. Acoustic velocity calculation method of oil tubing casing annulus based on all-phase FFT. Tech Acoust. 2021;40(02):246–53. (In Chinese).
12. Liang X, Zhang Z. Research on depth of oil well moving liquid surface based on short-term energy and LSTM. Comput Mod. 2021;4:15–19,26. (In Chinese).
13. Wang L, Wei Y, Wang Y, Chen Q, Liu P, Chai X. Research on comprehensive and effective acoustic signal processing methods for caculating downhole liquid level depth. Measurement. 2022;199:111452. doi:10.1016/j.measurement.2022.111452.
14. Chen Y, Sun T, Yang J, Chen X, Ren L, Wen Z, et al. Prediction of mud weight window based on geological sequence matching and a physics-driven machine learning model for pre-drilling. Processes. 2025;13(7):2255. doi:10.3390/pr13072255.
15. Roy BK, Santhosh KV. An intelligent instrument for measuring liquid level. In: Proceedings of the 2011 International Conference on Process Automation, Control and Computing; 2011 Jul 1–3; Coimbatore, India. New York, NY, USA: IEEE; 2011. p. 1–5. doi:10.1109/PACC.2011.5978861.
16. Bagheri H, Mohebian R, Moradzadeh A, Olya BA. Pore size classification and prediction based on distribution of reservoir fluid volumes utilizing well logs and deep learning algorithm in a complex lithology. Artif Intell Geosci. 2024;5(4):100094. doi:10.1016/j.aiig.2024.100094.
17. Cheng J, Yu D, Yang Y. Research on the intrinsic mode function (IMF) criterion in EMD method. Mech Syst Signal Process. 2006;20(4):817–24. doi:10.1016/j.ymssp.2005.09.011.
18. Nazari M, Sakhaei SM. Successive variational mode decomposition. Signal Process. 2020;174:107610. doi:10.1016/j.sigpro.2020.107610.
19. Kolokolov AS, Lyubinskii IA. Measuring the pitch of a speech signal using the autocorrelation function. Autom Remote Control. 2019;80(2):317–23. doi:10.1134/S0005117919020097.
20. Wu Y, Huang J, Xia J. AMDF-based pulse period detection improved algorithm. Comput Appl Softw. 2014;31(6):52–4. (In Chinese).
21. Davis RS. Equation for the determination of the density of moist air (1981). Metrologia. 1992;29(1):67–70. doi:10.1088/0026-1394/29/1/008.
22. Tsilingiris PT. Thermophysical and transport properties of humid air at temperature range between 0 and 100°C. Energy Convers Manag. 2008;49(5):1098–110. doi:10.1016/j.enconman.2007.09.015.
23. Li B, Martin EB. An approximation to the F distribution using the chi-square distribution. Comput Stat Data Anal. 2002;40(1):21–6. doi:10.1016/S0167-9473(01)00097-4.